View metadata, citation and similar papers at core.ac.uk
brought to you by CORE
provided by University of Queensland eSpace

The Astrophysical Journal, 518:L123–L126, 1999 June 20
© 1999. The American Astronomical Society. All rights reserved. Printed in U.S.A.

CHARACTERISTICS OF MAGNETOHYDRODYNAMIC OSCILLATIONS OBSERVED WITH THE MICHELSON DOPPLER IMAGER

A. A. Norton[1] and R. K. Ulrich
Department of Physics and Astronomy, University of California at Los Angeles, Los Angeles, CA 90095-1562
R. I. Bush
W. W. Hansen Experimental Physics Laboratory, Center for Space Science and Astrophysics, Stanford University, Stanford, CA 94305
and
T. D. Tarbell
Lockheed Martin Corporation, Solar and Astrophysics Laboratory, 3251 Hanover Street, Palo Alto, CA 94304
Received 1998 December 18; accepted 1999 April 22; published 1999 May 28

ABSTRACT

We report on the spatial distribution of the magnetogram oscillatory power and the phase angles between velocity and magnetogram signals as observed with the Michelson Doppler Imager. The data set is 151.″25 × 151.″25, containing the sunspot from 1997 December 2 with a temporal sampling interval of 60 s and spatial sampling of 0.″605. The simultaneously observed continuum intensity and surface velocity accompany the magnetic information. We focus on three frequency regimes: 0.5–1.0, 3.0–3.5, and 5.5–6.0 mHz, corresponding roughly to timescales of magnetic evolution, *p*-modes, and the 3 minute resonant sunspot oscillation. Significant low-frequency magnetogram power is found in lower flux pixels, 100–300 G, in a striking ring with filamentary structure surrounding the sunspot. The 5 minute magnetogram power peaks in extended regions of flux that measure 600–800 G. The 3 minute oscillation is observed in the sunspot umbra in pixels whose flux measures 1300–1500 G. Phase angles of approximately −90° between velocity and magnetic flux in the 3.0–3.5 and 5.5–6.0 mHz regimes are found in regions of significant cross amplitude.

Subject headings: MHD — Sun: magnetic fields — Sun: oscillations

1. INTRODUCTION

The interactions of photospheric magnetic fields with the motions of solar plasma is described by magnetohydrodynamics (MHD). Ionson (1978) recognized that acoustic waves perturbing the base of magnetic fields can generate MHD waves. Significant amounts of literature exist that address the theoretical generation and propagation of MHD modes in the solar atmosphere. The previous identification of oscillatory modes in sunspots from velocity and intensity measurements is not sufficient since MHD modes require simultaneous magnetic field and velocity information. Observational support of solar MHD modes is sparse (Ulrich 1996; Horn, Staude, & Landgraf 1997; Norton et al. 1998; Lites et al. 1998; Rüedi et al. 1998).

Although many MHD waves may exist, two main mechanisms alter the measured magnetic flux: (1) the bending of field lines and (2) the compression of field lines. Under simplified conditions, the bending mode corresponds to an Alfvén wave, and a compressional mode corresponds to a magnetoacoustic wave. The observational tendency to image active regions at disk center may have historically hindered Alfvén wave detection. The measurement of δB due to a change in direction is easier to detect in transverse fields than in line-of-sight fields. It is easier to detect bending modes at the limb and compressional modes at disk center.

MHD waves are a prime coronal heating candidate. Suggested MHD wave dissipation processes are phase mixing (Heyvaerts & Priest 1983) and resonant absorption (Davila 1987). Detection of MHD oscillations is the first step toward understanding the role that MHD waves play in atmospheric energy transport.

[1] Visiting Scholar, Physics Department, University of Queensland, Brisbane, QLD 4072, Australia.

2. OBSERVATIONS

The Michelson Doppler Imager (MDI) instrument images the Sun at five different wavelengths centered around the mid-photospheric Ni I 6768 Å line. By obtaining filtergrams at the five wavelengths, we sample the line profile. The average of the left- (LCP) and right-circularly polarized (RCP) observed central wavelengths is the Doppler shift. A longitudinal magnetic flux indicator, uncorrected for observation angle, is measured by subtracting the observed central wavelengths of RCP images from LCP images. The continuum intensity is measured at a wavelength far from line center. We analyzed a 151.″25 × 151.″25 sunspot-centered region in the high-resolution field on 1997 December 2. The data set consists of 492 B, I_c, and v images; the snapshots are shown in lower panels of Figure 1. The region is tracked by adjusting heliographic coordinates of map centers as a function of time. The average center-to-limb angle of the sunspot center is 19.°77. The data are stored as three-dimensional data cubes, with sides of 250 × 250 pixels × 492 minutes.

3. ANALYSIS AND RESULTS

Temporal variations from individual pixels are analyzed without spatial averaging. The signals are de-trended using a Gaussian filter (30 minute width) before the average values are subtracted. The power spectra of the signals are computed. Three-dimensional data cubes are created where the temporal axis has been transformed into frequency. Averaging over the selected frequencies, we plot the spatial distribution of power for B, I_c, and v in Figure 1. The magnetogram power plotted in Figure 1 is normalized so that the noise, as measured in the 7.5–8.0 mHz high-frequency band, is unity. High-frequency power in the strongest magnetic flux regions is enhanced by instrumental effects due to reduced intensity and broader

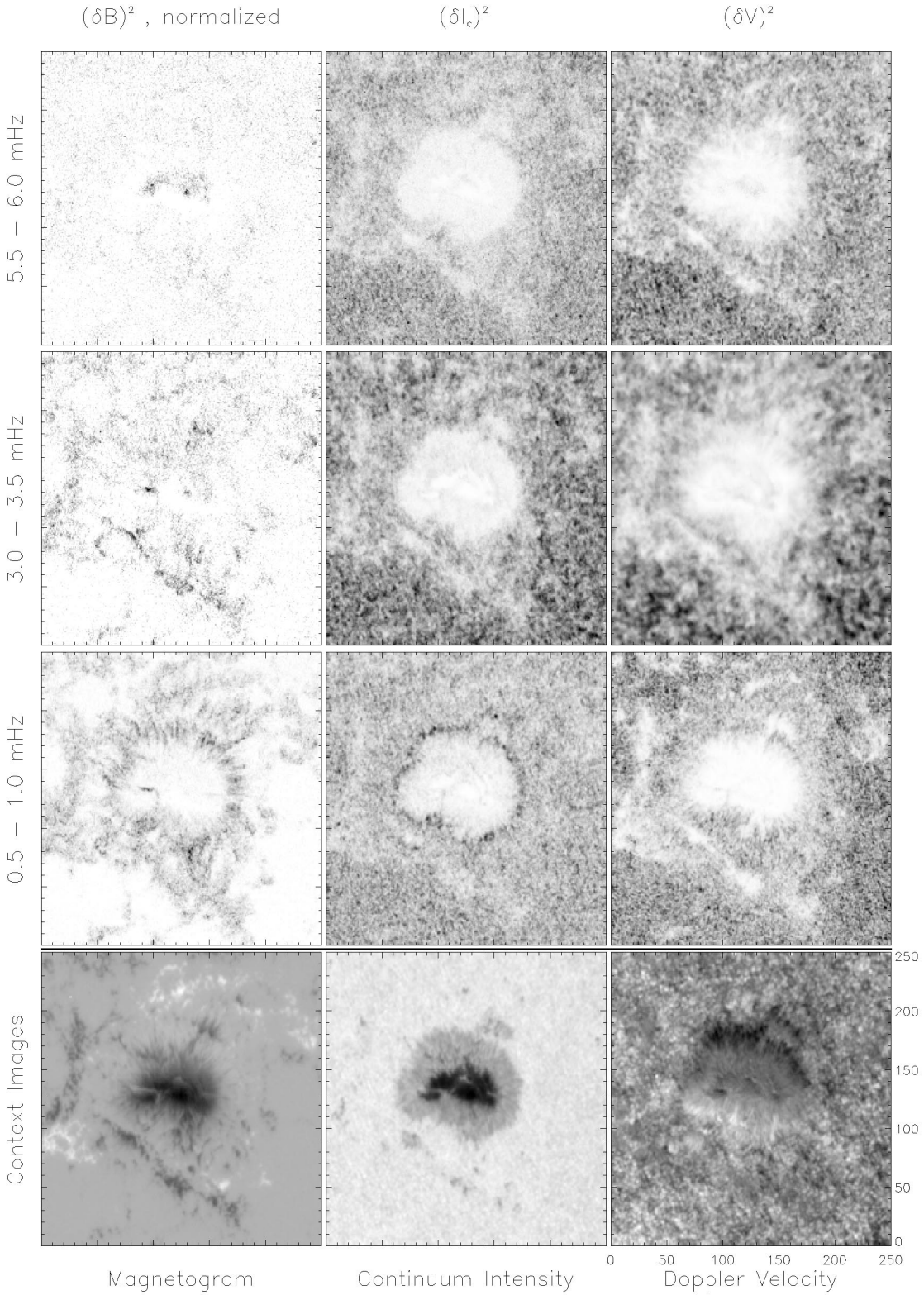

FIG. 1.—Context images and spatial distributions of power. *Rows from bottom*: Context images, 0.5–1.0, 3.0–3.5, and 5.5–6.0 mHz frequencies. The panels from left to right contain B, I_c, and v data. *Gray scales*: Black represents the maximum values, and white the minimum, but the I_c context image is reversed. The context images from left to right have maximum values of 2057 G, 3436, and 1.3 km s^{-1} and minimum values of -876 G, 658, and -1.3 km s^{-1}. The maximum values of power from the lower to upper plots are B: 1000, 220, and 178 normalized power units; I_c: 10445, 1690, and 280; and v: 53×10^3, 151×10^3, 10×10^3 (m s^{-1})^2. The minimum power values are B: 7.2, 8.4, and 6.9 normalized power units; I_c: 10, 3.2, and 2.2; and v: 153, 1650, and 70 (m s^{-1})^2.

absorption lines or by increased solar variations. We cannot distinguish between these options, but if the high-frequency power for these pixels is solar, our normalization could be incorrect.

Averaged magnetogram power spectra are plotted in Figure 2. Each signal is divided by its standard deviation. Then the 399 spectra from pixels whose absolute mean measured flux is within the ranges 100–300, 600–800, and 1300–1500 G are averaged and plotted in Figure 2. The ranges are selected because the low-frequency, *p*-mode, and 3 minute power peaked herein.

The cross amplitude and phase spectra for the selected frequency regimes are found in Figure 3. To compute the cross spectra, signals are interpolated onto a 10 s grid and shifted past each other in 10 s lag increments for up to a ± 15.16 minute period. The resulting cross covariance function is recorded. Restricting the lag interval to ensure a wave train coherence time is equivalent to applying a Bartlett window. The Fourier transform of the cross covariance function, the cross spectrum, is computed at each position. The cross amplitude and phase spectra are plotted in the left and right panels of Figure 3, respectively.

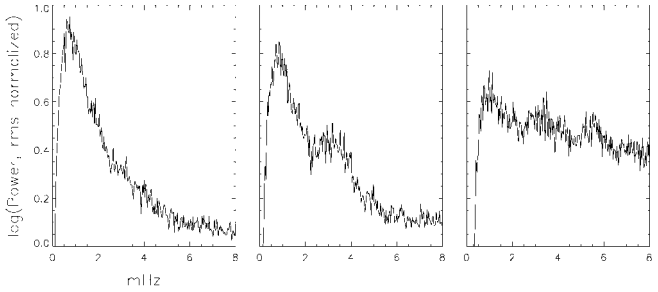

FIG. 2.—The logarithm of rms-normalized magnetic power is plotted as a function of frequency for pixels whose mean flux values are within the 100–300, 600–800, and 1300–1500 G ranges. The average standard deviation values used for signal normalization are 13.0, 14.3, and 15.9 G, respectively.

4. SPURIOUS CONTRIBUTIONS TO OSCILLATORY MAGNETIC SIGNAL

Attention is given to two effects that could mimic an oscillatory magnetic signal: (1) the misregistration of the LCP and RCP images and (2) the optical depth changes due to temperature fluctuations affecting the measurement height where magnetic field gradients, dB/dz, are present. To determine whether magnetogram oscillations have their origin in LCP-RCP image differences, misregistered data sets were simulated. The details of this analysis will follow in a subsequent publication. Let it suffice herein to note that spurious contributions due to misregistered images are most worrisome in quiet regions. In active regions, the suppression of v amplitudes decreases the cross talk between the v and B signals.

Opacity changes due to temperature fluctuations cannot be ruled out as a source of the spurious oscillatory magnetic signal without an indicator such as the thermal line ratios. The analysis of MDI flux estimates as a function of temperature will be presented in a subsequent publication. We acknowledge that cross talk into the δB signal from fluctuations in temperature, density, and other parameters may contribute to the magnetogram oscillations measured herein. Further research will determine what, if any, corrections are necessary to convert the magnetogram variation into a measure of the magnetic field strength variation.

5. DISCUSSION

Most significantly, the spatial distribution of magnetogram power is distinctly different in the three frequency regimes. Low-frequency buffeting and evolution occur around the sunspot and plage. Notable filamentary structure seen across the penumbra/quiet boundary intimates an advection of flux at low frequencies. Magnetogram oscillations on the 5 minute timescale are presumably the magnetic response to velocities already present in the photosphere. The 5 minute magnetogram oscillations in extended plage regions suggest that the plage environment may more readily convert acoustic waves into MHD waves. The 3 minute resonant sunspot oscillation is found in a portion of the umbra not associated with the strongest flux, but rather an area bounding the darkest part of the umbra.

The uneven spatial distribution of power would cause an investigation restricting its MHD wave search to the strongest flux areas to be unsuccessful. It is not yet clear what conditions are favorable for the generation of measurable MHD oscillations. Loop termination points or strong gradients in magnetic fields might be required. The power distribution and small-scale nature of the magnetic element do not lend themselves to spatial averaging. The power spectra shape seen in Figure 2 becomes flatter with increasing flux. Stronger fields evolve less, leveling the spectra at low frequency. The increase of high-frequency power in strong flux spectra is due to the reduced intensity and broader absorption lines or to the increased solar variation. The changing shape of the magnetogram spectra should be taken into account when comparing power from regions of differing B-values.

Some positions containing strong magnetic power at 3.0–3.5 mHz in Figure 1 do not show correspondingly high (v, $\delta|B|$) cross-amplitude values in Figure 3. This suggests the presence of different MHD modes or cross talk mechanisms. The mode with stronger line-of-sight velocity variations is more visible in the cross-amplitude plot.

Phase angles of approximately $-90°$ between (v, $\delta|B|$) signals can be interpreted as $\delta|B|$ reaching its maximum a quarter of a cycle before v. Phases of $-90°$ dominate regions of significant cross amplitude in the 5 and 3 minute bands. This phase relation is not a measure of magnetoacoustic waves in which v is expected to lead $\delta|B|$. Its interpretation is still uncertain, but Rüedi et al. (1999) demonstrate that $\delta|B|$ leading v a quarter of a cycle could be the result of measuring dB/dz during opacity changes. It appears that at least three different mechanisms (cross talk or others) dominate at different spatial positions, producing the phase structure seen in Figure 3. We will not know how the observational bias against detecting Alfvén waves at disk center affects phase determinations until a similar analysis can be conducted with limb data for comparison. The phase relations described by Ulrich (1996) may not apply in sunspots where the flux-tube model is inappropriate.

Temperature, density, and corresponding opacity variations may contribute to B amplitudes and phases through cross talk. Although the interpretation of the signal variation is complicated by the effects of cross talk, the cross talk is nonetheless of solar origin, so that the spectral power density maps provide a real measure of MHD oscillations. The distinct spatial dis-

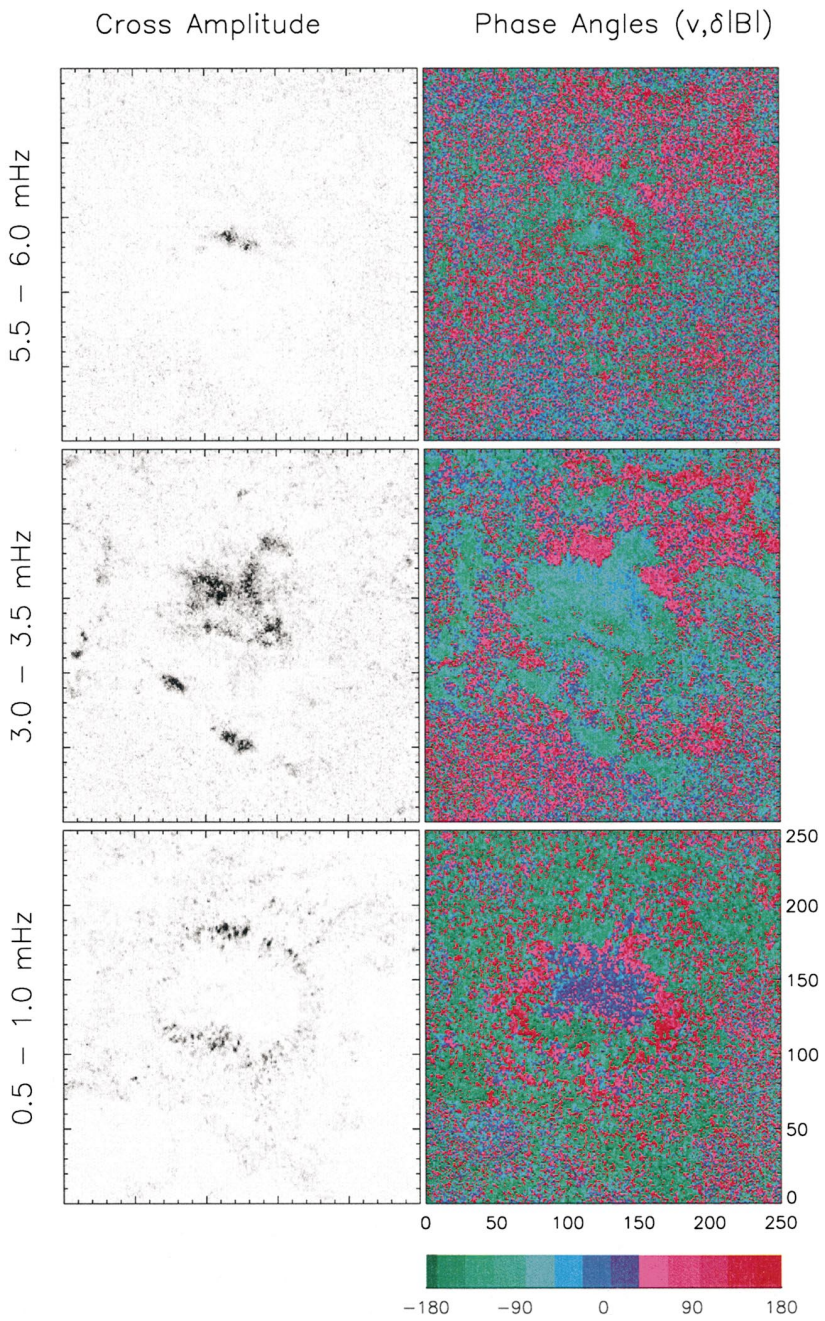

FIG. 3.—Cross amplitude (*left*) and phase spectra (*right*) are shown for the 0.5–1.0, 3.0–3.5, and 5.5–6.0 mHz regimes. The phase data are plotted for all spatial points, regardless of cross-amplitude significance, in order to display spatial structure of phases.

tribution of magnetogram power in the three frequency regimes can assist in the selection of regions for future MHD wave searches as well as in the numerical comparison of amplitude and phase measurements from other data sets.

REFERENCES

Davila, J. M. 1987, ApJ, 317, 514
Heyvaerts, J., & Priest, E. R. 1983, A&A, 318, 957
Horn, T., Staude, J., & Landgraf, V. 1997, Sol. Phys., 172, 69
Ionson, J. A. 1978, ApJ, 226, 650
Lites, B. W., Thomas, J. H., Bogdan, T. J., & Cally, P. S. 1998, ApJ, 497, 464
Norton, A. A., Ulrich, R. K., Bogart, R. S., Bush, R. I., & Hoeksema, J. T. 1998, in IAU Symp. 185, New Eyes to See inside the Sun and Stars, ed. F.-L. Deubner, J. Christensen-Daalsgaard, & D. Kurtz (Dordrecht: Kluwer), 453
Rüedi, I., Solanki, S. K., Bogdan, T., & Cally, P. 1999, in Solar Polarization, ed. K. N. Nagendra & J. O. Stenflo (Dordrecht: Kluwer), in press
Rüedi, I., Solanki, S. K., Stenflo, J. O., Tarbell, T., & Scherrer, P. H. 1998, A&A, 335, L97
Ulrich, R. K. 1996, ApJ, 465, 436